CTREC: C-arm Tracking and Reconstruction using Elliptic Curves

Gouthami Chintalapani[1], Ameet K. Jain[1,2], David H. Burkhardt[3], Jerry L. Prince[1], Gabor Fichtinger[1,4]
1- Johns Hopkins University; 2 - Philips Research North America;
3 - Haverford College, 4 - Queenś University

Abstract

C-arm fluoroscopy is ubiquitous in contemporary surgery, but it lacks the ability to accurately reconstruct three-dimensional information, attributable to the difficulty in obtaining the pose of X-ray images in 3D space. We propose a unified mathematical framework to address the issues of intra-operative pose estimation, correspondence and reconstruction, using simple elliptic curves. In contrast to other fiducial-based tracking methods, our method uses a single ellipse to constrain 5 out of 6 degrees of freedom of C-arm pose, along with randomly distributed unknown points in the imaging volume (either naturally present or induced by randomly placed beads or other markers in the image space) from two images/views to completely recover the C-arm pose. Preliminary phantom experiments indicate an average C-arm tracking accuracy of 0.51° *and* 0.12° *STD. The method appears to be sufficiently accurate and appealing for many clinical applications, since it uses a simple elliptic fiducial coupled with patient information and has very minimal interference with the workspace.*

1. Introduction

C-arm fluoroscopy is the most commonly used intra-operative imaging modality because of its low cost and ease of use, but it currently lacks the ability for robust and easy quantitative guidance. For intra-operative quantitative analysis, one needs to address the issues of 1) image distortion; 2) calibration of imaging parameters; 3) pose estimation; and 4) registration to other imaging modalities. The first two problems are well studied in literature and several solutions have been proposed to date [3, 14, 16]. On the other hand, pose recovery on unencoded mobile C-arms is still a major technical problem that presently does not have a practical solution in many areas of application. Adding to the problem is the non-isocentric nature of C-arms, where the two axes of rotation does not intersect. Also, it has been observed that calibration parameters, for both distortion and image, change from pose to pose, making it even harder to achieve accurate pose recovery.

To date, a wide variety of approaches have been proposed to recover C-arm pose, ranging from external tracking devices [12, 13], precise calibration fiducials consisting of beads, lines, conics etc in known geometry [3, 6, 11, 15, 16], to image-based pose estimation methods [5, 9] adapted from the computer vision literature. Auxiliary tracking devices are expensive and need an extra calibration step, optical systems have line of sight problems and electromagnetic trackers suffer from distortion from metallic instruments, thus adding to the complexity of the operating room.

Radio-opaque fiducials placed in the field of imaging have been demonstrated to be capable of achieving reasonable accuracies. However, these fiducials need to be manufactured and segmented precisely and the accuracies depend on the size of the fiducial, the number of features and the type of features, adding to the segmentation and imaging volume problems. It has been shown that ellipses serve as ideal features as a 3D ellipse would project as a closed ellipse in the 2D images [4, 6]. A circle is a special case of ellipse and has been used widely for pose estimation, either alone or with other features [2, 7, 10].

In image-based methods, point correspondences across the images, without the knowledge about their 3D locations, offer very strong constraints for determining the C-arm pose, popularly known as bundle adjustment in computer vision parlance[9]. Jain *et al.* proposed a mathematical framework to solve for pose parameters, point correspondences, and reconstruction using a high dimensional non-linear optimization with point features from three images [5]. It can be noticed that there is a trade-off between the number of points and the number of images used to determine the pose accurately. Determining correct point correspondences depends on the number of points, spacing between the points, configuration of the points and also on the number of images to eliminate degenerate matches. At the same time, increasing the number of images adds to the complexity of the non-linear optimization problem. While some procedures may be more tolerant to these shortcomings, despite pressing clinical needs, better approaches to achieve intra-operative quantitative fluoroscopy that fits

the existing clinical workflow are needed, thereby providing motivation for this work.

In this paper, we propose a unified framework to couple fiducial-based techniques with image-based algorithms to effectively determine C-arm pose from two or more images. We are using a single ellipse as our fiducial because ellipses serve as excellent 3D marker owing to their constrained mathematical framework and superior image segmentation, as reported in [6]. We present a detailed mathematical framework to recover pose using a known 3D ellipse and its 2D projective images. Our mathematical analysis shows that the ellipse from a single image offers symmetric solutions and hence can only constrain 5 out of 6 degrees of freedom. To recover all 6 degrees of freedom, we impose more constraints in the form of point correspondences across multiple images. It can be argued that these extra constraints can be obtained by adding more features to the elliptic fiducial for example a BB, a line, or even a second ellipse. Adding more features increases the burden of segmentation, interference with the anatomy and also creates a need for precise manufacturing and extra hardware in the operating room. Instead, we propose to use multiple projections and feature/point correspondences across these images to recover the pose, thereby using patient anatomical information as part of the fiducial. This is a novel method which benefits from both fiducial based methods and image based methods as the fiducial provides a good initial estimate for the point correspondences and the point correspondences in turn resolve the degenerate cases from the single ellipse.

We are targeting two pertinent applications for this work: 1) brachytherapy and 2) orthopaedics. Prostate brachytherapy is a procedure where radio-active seeds are implanted into the prostate to treat prostate cancer. C-arm fluoroscopy is used to get real-time dose analysis in the operating room [5]. Our framework fits well into this procedure as the ellipse has very minimal interference with the anatomy and at the same time we can also use the radioactive seeds as our point features to accurately determine the C-arm pose. Moreover, in orthopaedic applications, it is very common to insert screws, surgical markers etc., that can serve as our point fiducials. In applications that do not have many point features, one can either induce some markers or identify homologous landmark features in the projection images and use them as fiducials. All things considered, we believe that this combined approach has great potential for intra-operative C-arm tracking that would fit very well into existing clinical scenarios.

2. Method

The main components of this problem are: 1) c-arm pose and 2) point correspondences. It is assumed that the points have been segmented from the X-ray images. C-arm imaging is typically approximated as a 5-parameter pinhole perspective projection camera [3, 14, 16] to be calibrated intra-operatively for each individual image. Recently, however, it has been shown that precise C-arm calibration does not significantly improve pose reconstruction, especially the relative pose between the images [5]. We assume constant calibration across the images, along with known pixel sizes. We present a detailed framework to estimate C-arm pose using two images, though this framework can be easily extended to three or more images.

2.1. Pose Estimation using Single Ellipse

Given a known 3D ellipse, the goal here is to estimate the pose of this ellipse from its corresponding projective images. It is typical to represent the segmented 2D ellipse as an equation of the form:

$$Au^2 + Buv + Cu^2 + Du + Fv + G = 0 \qquad (1)$$

in each image, in which u and v are respectively the coordinates along the x and y axis of the image, measured in pixels, and A, B, C, D, F, and G are constants determined by the segmentation algorithm. It can be observed that this correlates with the general equation of a conic, the origin of which is sitting at the principal point. The equation of such a cone will appear like

$$A_0x^2 + B_0xy + C_0x^2 + \frac{D_0}{f}xz + \frac{F_0}{f}yz + \frac{G_0}{f^2}z^2 = 0. \quad (2)$$

where x, y, z are coordinates in a frame that has the focal point of the x-ray device as origin with z axis perpendicular to the image plane and x and y axis parallel to the imaging plane, and f is the focal length of the imaging scenario. This equation can be represented in matrix form as

$$\begin{bmatrix} x & y & z \end{bmatrix} \begin{bmatrix} A_0 & \frac{B_0}{2} & \frac{D_0}{2f} \\ \frac{B_0}{2} & C_0 & \frac{F_0}{2f} \\ \frac{D_0}{2f} & \frac{F_0}{2f} & \frac{G_0}{f^2} \end{bmatrix} \begin{bmatrix} x \\ y \\ z \end{bmatrix} = 0. \quad (3)$$

which can also be represented as

$$XM_0X^T = 0. \qquad (4)$$

We broke the process into several steps using a method similar to that described for the case of a circle by Costa and Shapiro [2] and the detailed derivation can be found in [1]. We assume for simplicity that the coordinate frame of the 3D ellipse has the x-axis along its major axis, the y-axis along its minor axis, and the origin in the center of the ellipse. The first step involves finding the rotation between the coordinate frame defined by the image plane and the base coordinate frame of the cone itself (with x and y axes along

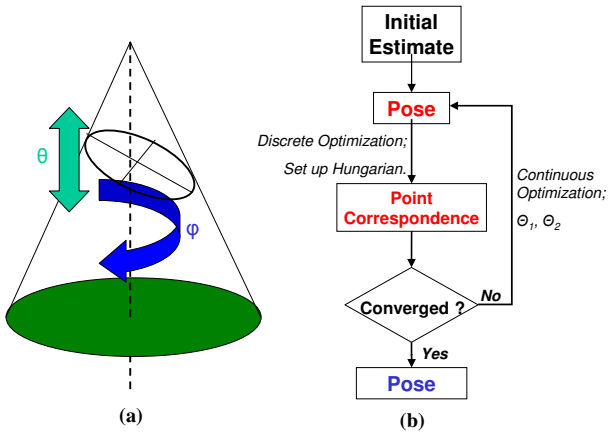

Figure 1. Graphical representation of the angles phi and theta, used to slice the cone and obtain an ellipse(left). Algorithmic flowchart showing pose estimation with point correspondences (right)

the major and minor axis of the cone and z axis along the cone's center). Note that the rotation matrix that achieves this transformation is just the eigenvectors of the original cone matrix M_0. The base frame of the cone is of particular interest because in it the cone equation has special form of the type

$$\begin{bmatrix} x & y & z \end{bmatrix} \begin{bmatrix} A_B & 0 & 0 \\ 0 & C_B & 0 \\ 0 & 0 & \frac{G_B}{f^2} \end{bmatrix} \begin{bmatrix} x \\ y \\ z \end{bmatrix} = 0 \quad (5)$$

The next step is to find the transformation between the coordinate frame of the base cone and that of the 3D ellipse. By applying the constraints imposed by the physical size of the ellipse, we attempt to evaluate the set of transformations that would achieve this for a given image. We parameterize the problem by defining two values, ϕ and θ which together can represent a rotation from the base frame (z-axis aligned with the cone) to an arbitrary frame. To model this transformation, the base frame is first rotated by ϕ about its z axis and then by θ around the new y-axis. This transformation is illustrated in Figure 1a.

For any image, there are infinitely many possible (ϕ, θ) combinations, corresponding to infinitely many physical ellipses that could generate the observed projected ellipse in the X-ray image. These rotations can be expressed by the following matrices:

$$R_\phi = \begin{bmatrix} \cos\phi & -\sin\phi & 0 \\ \sin\phi & \cos\phi & 0 \\ 0 & 0 & 1 \end{bmatrix} \quad (6)$$

$$R_\theta = \begin{bmatrix} \cos\theta & 0 & \sin\theta \\ 0 & 1 & 0 \\ -\sin\theta & 0 & \cos\theta \end{bmatrix} \quad (7)$$

Our goal therefore is to solve for ϕ and θ such that:

$$X R_\phi R_\theta M_P R_\theta^T R_\phi^T X^T = 0 \quad (8)$$

where M_P is the equation for the cone in its base frame.

Furthermore, note that all parallel planes slicing the cone, create a conic curve with the exact same eccentricity. In our case, this eccentricity should be equal to the eccentricity of the 3D ellipse (a known constant). So without loss of generality, if we set $Z = 1$, we will get the equation of an ellipse, such as

$$A_P * x^2 + B_P * xy + C_P * y^2 = K \quad (9)$$

where

$$A_P = G_0 \sin^2\theta + C_0 \cos^2\theta \sin^2\phi + A_0 \cos^2\theta \cos^2\phi \quad (10)$$

$$B_P = 2\{-A_0 \cos\theta \cos\phi \sin\phi + C_0 \cos\theta \sin\phi \cos\phi\} \quad (11)$$

$$C_P = A_0 \sin^2\phi + C_0 \cos^2\phi \quad (12)$$

The ellipse generated in this slice can also described by a more common equation:

$$\frac{(x\cos\psi + y\sin\psi)^2}{a^2} + \frac{(x\sin\psi - y\cos\psi)^2}{b^2} = K \quad (13)$$

where ψ is a rotation around the z-axis of the 3D ellipse, a & b are the major & minor axes of the 3D ellipse. K will be scale-constant dependent on the z value at which the slice was taken. Expanding this equation simplifies to

$$\left(\frac{\cos^2\psi}{a^2} + \frac{\sin^2\psi}{b^2}\right) x^2 + \sin 2\psi \left(\frac{1}{a^2} - \frac{1}{b^2}\right) xy + \left(\frac{\sin^2\psi}{a^2} + \frac{\cos^2\psi}{b^2}\right) y^2 = K \quad (14)$$

So, from equation 9, we know that for some angle of rotation ψ:

$$A_P = \left(\frac{\cos^2\psi}{a^2} + \frac{\sin^2\psi}{b^2}\right)$$

$$B_P = \sin 2\psi \left(\frac{1}{a^2} - \frac{1}{b^2}\right)$$

$$C_P = \left(\frac{\sin^2\psi}{a^2} + \frac{\cos^2\psi}{b^2}\right)$$

Combining these equations to eliminate ψ and K, gives us

$$A_P + C_P = K\left(\frac{1}{a^2} + \frac{1}{b^2}\right)$$

$$(A_P - C_P)^2 + B_P^2 = K^2\left(\frac{1}{a^2} - \frac{1}{b^2}\right)^2$$

$$\implies \frac{(A_P - C_P)^2 + B_P^2}{(A_P + C_P)^2} = \frac{(\frac{b^2}{a^2} - 1)^2}{(\frac{b^2}{a^2} + 1)^2}$$

Note that if we were imaging a circle, the right hand term reduces to 0, indicating $B_P = 0$, and $A_P = C_P$. Substituting the values for A_P, B_P, and C_P previously presented in equations 10, 11, 12 allows us to obtain an equation relating θ to ϕ. This equation is a quadratic equation in $cos^2(\phi)$ of the form, with the $K_n(\theta)$ functions of θ:

$$K_1(\theta)\cos^4\phi + K_2(\theta)\cos^2\phi + K_3(\theta) = 0 \qquad (15)$$

Since equation 15 is a bi-quadratic equation in $cos\phi$, for any given value of θ there are 8 values of ϕ in general that satisfy the constraint that it imposes. Moreover, observe that if ϕ ($0 \leq \phi < \pi/2$) is a solution, then $\pi - \phi$, $-\pi + \phi$ & $-\phi$ are also solutions. These would correspond to the 4 symmetric solutions owing to the inherent symmetry in the cone and the ellipse. Furthermore, ϕ and $-\pi+\phi$ correspond to the same ellipse sitting in exactly the same position. In many cases, some solutions for ϕ would be imaginary when $|cos\phi| > 1$, meaning that there is no feasible ellipse for that given θ.

At this stage, we have constrained the solution space of the ellipse/C-arm pose, reducing the 6-dimensional pose-parameter space to a function of a single parameter ϕ/θ. With respect to the ellipse frame, there are eight symmetric locations of the X-ray source, all of them being reflections along the x-y, y-z and z-x planes. The other eight solutions have the same position of the X-ray source, but the image rotated by π along the center line of each 3D cone. Thus it can be observed that, with respect to the ellipse, all the feasible pose solutions lie on 8 non-intersecting closed curves parametrized by ϕ/θ.

Given a (ϕ, θ) combination, to obtain the third rotation angle ψ we apply the following transformation to our coordinate frame, giving us a cone of the form

$$XR_\phi R_\theta M_P R_\phi^T R_\theta^T X^T = XC_E X^T = 0 \qquad (16)$$

where C_E is the cone equation in a coordinate frame aligned with the frame of the 3D ellipse, and a rotation of ψ along its z-axis. We next apply a rotation by the angle ψ to bring the x and y axes of our coordinate system parallel to the major and minor axes of the real ellipse. Solving the equation, this angle is given by

$$\psi = 1/2 * \arctan(2 * B_E/(C_E - A_E)) \qquad (17)$$

The rotation transformation of ψ along the z-axis can be described as

$$R_\psi = \begin{bmatrix} \cos\psi & -\sin\psi & 0 \\ \sin\psi & \cos\psi & 0 \\ 0 & 0 & 1 \end{bmatrix} \qquad (18)$$

The coordinate system created by the combination of these rotations now has axes parallel to the axes of the 3D ellipse, but is centered at the imaging focal point. The final step therefore, is to compute the translation required to bring the center of the frame to the center of the ellipse. This translation is computed by taking a slice of the cone at distance f away from the center, computing its major axis at this point. Equating the computed length of the major axis as a function of f, to the known value, provides f. The coordinate system is then translated by this vector.

Combining these transformations allows us to create an algorithm to determine the set of possible poses that could have created a given image. However, as infinitely many possible (ϕ, θ) combinations exist, the ellipse image cannot be used to uniquely determine the pose. It constrains 5 of the 6 degrees of freedom of pose, allowing a single degree of freedom that must be removed through further constraints.

2.2. Combined Mathematical Framework

As shown above, a single ellipse from each projection image returns the pose in (ϕ, θ) space with 8 degenerate poses, i.e., the projection of the known 3D ellipse in any of these poses would result in exactly the same 2D image. In order to eliminate these degenerate cases, we propose to impose more constraints in the form of point correspondences across images. Even though the projections of the 3D ellipse are identical, the projections of the 3D point clouds differ and hence provides us with extra constraints to break the symmetry as shown below.

Let N_m be the number of points identified in images I_m with pose $[R_m, T_m]$, θ_m be the corresponding solution space for C-arm pose using ellipse from image I_m and projection model M_m. Let s_{lm} be the position of l^{th} segmented point in m^{th} image. When two images are used, the optimization problem can be formulated as follows:

$$\underset{\theta_1, \theta_2, f}{\arg\min} \quad \sum_{i=1}^{N_1}\sum_{j=1}^{N_2} \mathcal{C}_{ij} f_{ij}$$

where

$$\sum_{j=1}^{N_2} f_{ij} \geq 1 \; \forall \, i; \sum_{i=1}^{N_1} f_{ij} \geq 1 \; \forall \, j; f_{ij} \in \{0, 1\} \qquad (19)$$

and $\mathcal{C}_{ij}$ is the the cost of matching point p_{i1} to points p_{j2}. Note that it varies with any variation in θ_1, θ_2. f_{ij} is a discrete variable taking a value $1/0$, and deciding the correctness of the match $\langle i, j \rangle$. The inequalities force every segmented point to be chosen at least once. Thus, f represents any feasible global match (and vice versa), with the cost of that correspondence given by $\sum\sum \mathcal{C}_{ij} f_{ij}$. The problem hence is to compute θ_1, θ_2, f that minimize the total cost. It should be noted that since the images represent

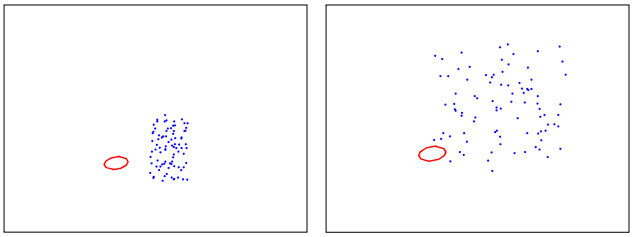

Figure 2. Simulated point clouds along with ellipse fiducial for prostate brachytherapy and orthopaedic procedures

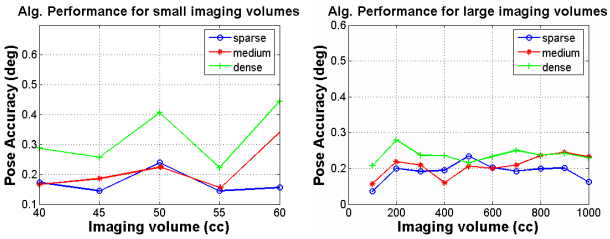

Figure 3. Relative pose error as a function of the imaging volume for small volumes(left) and large volumes (right)

a real situation, this optimization has a solution with a near-zero cost. The procedural flow diagram is shown in Figure 1b. For each θ_i, there are eight ϕ_i symmetric solutions and hence we evaluate the objective function 64times for two images to eliminate the degenerate cases. The number of evaluations can be decreased by tailoring the algorithm to be application dependent or by constraining the motion of the C-arm etc. The basic idea is that at global optimum, correct pose would invoke correct correspondences and these correspondences would converge to the optimal pose. At any other point in the solution space, incorrect pose would lead to inconsistent correspondences and hence by iteratively solving for both pose and point correspondences, a unique global solution can be achieved.

In general, any cost metric that globally measures the deviation from the observation, should perform well. We use projection error as our cost metric. This projection error can be computed as the L_2 norm of the projection of the 3D points (computed by intersecting the rays from the corresponding 2D points in the X-ray image to its source) on to the 2D images. Once the cost matrix is computed, we use traditional Hungarian assignment method to solve for optimal point correspondences [8].

3. Experiments and Results

Simulation Studies: Two types of synthetic data, one for prostate brachytherapy and the other for orthopaedic applications, were created to evaluate our algorithm. Both the simulation software and the algorithm were implemented in MATLAB. For two images, the algorithm takes about 20-60 seconds depending on the number of points used, with typical convergence in 2-3 iterations. The C-arm imaging parameters for both the simulations are: focal length = 1000 mm; pixel size = 0.44 mm/pixel; image size = (512, 640); and origin = (256, 320); The diameter of the shaft of 3D ellipse was fixed at 30 mm and the ellipse itself is oriented at an angle of 30° along the shaft. For prostate brachytherapy simulations, we created 5 datasets, each dataset has 6 images taken at regular intervals along a 20° cone. We varied the imaging volume from $40cc$ to $60cc$ in increments of $5cc$. For orthopaedic data, we varied the imaging volume from $100cc$ to $1000cc$ in increments of $100cc$. We divided the experiments into three separate cloud sizes: *sparse*, *medium*, and *dense* clouds consisting of atleast 10–15, 20–30, and 70–80 points respectively. These point clouds were chosen randomly for 5 iterations. Figure 2 shows an example simulated image with ellipse and point clouds. We believe that this data represents the spectrum of different types of surgical scenarios including brachytherapy and orthopaedic procedures.

Figure 3 shows the simulation results for small and large imaging volumes. Each datapoint is an average of $5 * \binom{6}{2} * 5 = 375$ runs. Pose recovery accuracy varies with the size of the point cloud, average being about 0.34° for small volumes and 0.2° for large volumes. Although, the variation is not much significant with the large volumes because of the wide distribution of the feature points. These results show that when there is no error in the data, pose can be recovered accurately.

We are currently exploring the sensitivity of the algorithm to the segmentation errors from both ellipse segmentation and point segmentation. The overall failure rate for large imaging volumes has decreased from 10% to 0.1% when compared to the small imaging volumes. These simulation results show that our algorithm successfully converges to the optimal solution in case of large imaging volumes and small imaging volumes with sparse and medium data distribution and is near perfect (success rate of 95%) for small imaging volumes with dense data points. This can be attributed to the fact that the point mismatches are more prevalent in dense point clouds and hence are throwing off the convergence in the two image algorithm. We show an improvement in the performance by using partial information from the third image below.

Phantom Experiments: Experiments were performed on a brachytherapy phantom consisting of both the seeds and the FTRAC fiducial rigidly attached as shown in Figure 4. The cloud phantom comprises of multiple slabs, thus capable of multiple *random* point configurations. 100 points with 1.56 $points/cc$ were used. X-ray images within a 20^o cone around the AP-axis were *randomly* taken using a *Philips Integris V3000* fluoroscope and corrected for distortion. Thus both the seed locations and X-ray pose were

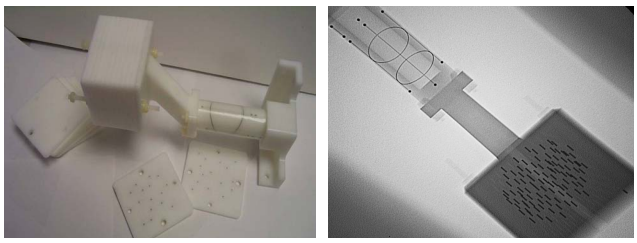

Figure 4. An image of the point phantom attached to the FTRAC fiducial (left). A typical X-ray image of the combination (right)

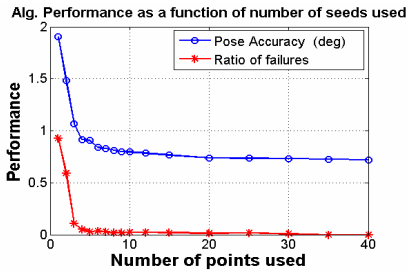

Figure 5. Performance as a function of number of points used along with the ellipse. Note that three to five points achieve 99% success rate.

not biased/optimized in any way, closely representing an uncontrolled surgical scenario. Each image was hand segmented to establish the true segmentation and correspondence, thereby allowing for some segmentation error. The true C-arm pose and reconstruction was compared to that computed from the algorithm.

Figure 5.b shows the performance of the algorithm with respect to the number of points used along with the ellipse. Each datapoint is an average of $5 * \binom{6}{2} * 30 = 2250$ runs. For phantom data, as few as $4 - 5$ points along with the ellipse are sufficient to accurately recover the pose (0.74°) and also are able to attain a success rate of 99%. The second set of phantom experiments involve taking multiple x-ray images and reconstructing the 3D seed locations from its corresponding 2D projection coordinates, for which accurate C-arm tracking is a must. For each phantom dataset, we have used sets of two images, determined the relative pose between these images and then reconstructed the 3D seed coordinates. Although this works perfectly on sparse data, our goal is to make it work on dense data such as brachytherapy seed data. The results are shown in Table 1. Note that the data in each cell is an average of 15 runs. Eventhough the average pose error is about (1°), only half of the seeds are correctly matched because of the reconstruction singularities introduced by using only two images, which is fully expected for dense data.

To understand better, how information from the third image enhances the algorithm convergence, we have used a third image to identify the correct matches as valid correspondences between the points identified by points that create loops of size one. Given two images, I_1, I_2, we select a third image I_3 and run the algorithm on sets of two images. Consider a point p_{i1} in image I_1 being matched to a point p_{j2} in image I_2, and to a point p_{k3} in image I_3. This match between p_{i1} to p_{j2} is considered a valid match if and only if p_{j2} matches p_{k3}. The pose estimation algorithm is run again using only these valid matches. We refer to this experiment as 2.5 images rather than 3 images in Table 1, since only partial information from the third image is used.

This added information from the third image has increased the matching rate to 90% with a better pose and reconstruction accuracy. The error for mismatched seeds is still high. The reason is that inspite of high matching rate and improved reconstruction accuracy, the projection of the solution using three images is not exactly the same as that of using two solutions. Although these accuracies are mostly acceptable, prostate brachytherapy needs 99% matching rate to determine the intra-operative dosage accurately, which can be achieved by extending our framework to use three images. The basic idea here would be to use two images to optimize the pose and then use three images to solve for matching iteratively. The theoretical complexity of using three or more images is similar to that of two images, except that the matching algorithm would be employing more sophisticated combinatorial checks like MARSHAL [5].

4. Discussion

A unified mathematical framework for C-arm tracking, point correspondences and reconstruction has been proposed, along with experimental validation on simulation and phantom studies. Our experiments indicate an average accuracy of 0.51° in orientation, with a STD of 0.12°. The primary contribution of this work is the use of ellipse to determine pose with a combinatorial approach to establish point correspondences. We show that the projection of elliptic curves constrains 5 out of the 6 degrees of freedom of the C-arm pose. Furthermore it can also recover the 3D scale of the reconstruction. To completely recover the true C-arm pose, our method uses constraints in the form of additional point correspondences from multiple images. We show that four or five additional correspondences can successfully recover the pose 99% of the time with an accuracy of 0.74°.

We have conducted our validation on randomly selected views and number/distribution of points, indicating the robustness of the algorithm to uniformity and reliability in performance. Though the alternatives of well designed calibration fixtures and image based procedures are also available, they become cumbersome and impractical, specifically when employed in the current clinical setup. We believe that the presented framework represents a significant

	Number of Seeds									
	2 Images					2.5 Images				
	40	**55**	**70**	**85**	**100**	**40**	**55**	**70**	**85**	**100**
Pose Accuracy (deg)	0.81	1.01	0.95	1.37	0.80	0.49	0.42	0.56	0.59	0.48
Matching Rate (%)	63.38	62.42	53.04	40.94	45.20	94.16	90.25	90.14	88.57	89.37
Reconstruction Error (matches)(mm)	3.27	1.27	1.72	3.84	1.18	0.19	0.25	0.33	0.22	0.31
Reconstruction Error(mismatches) (mm)	26.25	34.96	35.41	31.04	33.04	0.63	5.04	5.19	6.38	6.06

Table 1. The algorithm's performance on phantom data. 2-image seed matching is completely erroneous (left), with over a quarter of the seeds being mismatched with high reconstruction error, yet low projection error and reconstruction accuracy. Adding just little information from a third image boosts performance (right). Most seeds match, though the reconstruction error is high for the few mismatched seeds.

step toward a complete pose reconstruction system employing very little external hardware and very minimal interference with the anatomy being imaged (one could think of a small ellipse attached to a wire frame into the field of view and imaged along with the patient). Moreover, our simulation results show that this method can be used for a variety of applications ranging from prostate brachytherapy (small imaging volume, dense point features) to orthopaedic applications (large imaging volume, sparse to medium point features).

We are currently performing more simulations to validate the sensitivity of the algorithm to segmentation errors and are also looking at measuring target registration error distribution of the point clouds. Efforts to validate our system on clinical prostate brachytherapy data are currently underway. Further extension of this approach to reconstruct points using three views could significantly improve the current clinical viability of intra-operative quantitative fluoroscopy, especially in brachytherapy.

Acknowledgments

Supported by DoD PC050170, DoD PC050042 and NIH 2R44CA099374.

References

[1] D. Burkhardt, A. Jain, and G. Fichtinger. A cheap and easy method for 3D C-arm reconstruction using elliptic curves. In *Medical Imaging 2007: Visualization and Image-Guided Procedures. Edited by Cleary, Kevin R.; Miga, Michael I.. Proceedings of the SPIE, Volume 6509, pp. 65090B (2007).*, volume 6509 of *Presented at the Society of Photo-Optical Instrumentation Engineers (SPIE) Conference*, Mar. 2007.

[2] M. Costa and L. Shapiro. 3d object recognition and pose with relational indexing. *CVIU*, 79(3):364–407, September 2000.

[3] R. Hofstetter, M. Slomczykowski, M. Sati, and L. Nolte. Fluoroscopy as an imaging means for computer-assisted surgical navigation. *Comput Aided Surg*, 4(2):65–76, 1999.

[4] R. Hu and Q. Ji. Camera self-calibration from ellipse correspondences. In *ICRA*, pages 2191–2196, 2001.

[5] A. Jain and G. Fichtinger. C-arm tracking and reconstruction without an external tracker. In *MICCAI*, pages 494–502, 2006.

[6] A. Jain, T. Mustufa, Y. Zhou, E. C. Burdette, G. Chirikjian, and G. Fichtinger. A robust fluoroscope tracking (ftrac) fiducial. *Med Phys*, 32(10):3185–98, Oct 2005.

[7] F. Kahl and A. Heyden. Using conic correspondence in two images to estimate the epipolar geometry. In *ICCV*, pages 761–766, 1998.

[8] H. W. Kuhn. The Hungarian method for the assignment problem. *Naval Research Logist. Quart*, 2:83–97, 1955.

[9] Y. Ma and et al. *An Invitation to 3-D Vision*. Springer, 2000.

[10] P. K. Mudigonda, C. V. Jawahar, and P. J. Narayanan. Geometric structure computation from conics. *Lancet. Oncol.*, 4:233–241, 2002.

[11] N. Navab, A. Bani-Hashemi, M. Mitschke, D. W. Holdsworth, R. Fahrig, A. J. Fox, and R. Graumann. Dynamic geometrical calibration for 3-d cerebral angiography. In *SPIE Medical Imaging*, pages 361 – 70, Feb 1996.

[12] OEC 9800 FluoroTrak™. GE Healthcare, Waukesha, WI.

[13] StealtStation®. Medtronic Surgical Navigation Technologies, Louisville, CO.

[14] T. Tang. Calibration and point-based registration of fluoroscope images. Master's thesis, Queen's University, Jan 1999.

[15] Z. Yaniv and L. Joskowicz. Precise robot-assisted guide positioning for distal locking of intramedullary nails. *IEEE Trans Med Imaging*, 24(5):624–35, May 2005.

[16] J. Yao, R. H. Taylor, R. P. Goldberg, R. Kumar, A. Bzostek, V. R. Van, P. Kazanzides, and A. Gueziec. A c-arm fluoroscopy-guided progressive cut refinement strategy using a surgical robot. *Comput Aided Surg*, 5(6):373–90, 2000.